

Facile synthesis of GO/ZnO–Ag nanocomposite and evaluation of rhodamine B dye under sun light

P. Govindhan¹ · C. Pragathiswaran¹ · M. Chinnadurai²

Received: 3 June 2016 / Accepted: 8 August 2016 / Published online: 1 September 2016
© Springer Science+Business Media New York 2016

Abstract Graphene oxide (GO) composite photocatalysts are prepared by a combined impregnation chemical reduction method. GO composite used as a photo catalyst for the removal of organic pollutants and water purification system, it is due to the high surface area to volume ratio of redox potential of GO. The synthesised GO was nanocomposite with ZnO and Ag NPs by sol–gel method and developed as nanocatalysts. Band gap of GO nanocomposite was characterized by UV–visible diffuse reflectance spectroscopy (DRS). Fourier transforms infrared spectroscopy (FT-IR), powder X-ray diffraction (XRD), Field emission scanning electron microscope (FE-SEM), energy dispersive X-ray spectroscopy (EDAX) and transmission electron microscope (TEM). The XRD analysis also confirms the presence of Ag NPs of GO/ZnO–Ag nanocomposite. The GO/ZnO–Ag nanocomposite was used in the photocatalytic degradation of rhodamine B (RhB) dye under direct sunlight measured by UV–visible spectroscopy. The Ag NPs uniformly surface covers the surface of GO/ZnO nanocomposite result demonstrates the exceedingly improved the photocatalytic action. The superior photocatalytic activity of RhB dye degradation efficiency of 94 % was achieved. The presence of Ag NPs–GO/ZnO nanocomposite shows increasing photocatalytic activity due to its surface plasma resonance behaviour.

1 Introduction

Graphene oxide (GO) is a single layer sp^2 carbon atoms forcefully packed arrangement for unique two dimensional, rising star material and honeycomb structures [1–3]. It has been extremely attractive by a lot of applications, due to its excellent mechanical, thermal stability, optoelectronic properties [4, 5]. GO is a planar structure, high thermal conductivity, excellent mobility of electron charges at room temperature, high specific surface area, large scale and low cost [6–9]. The most important dispute in the preparation of graphene is to overcome the physically powerful exfoliation energy of the stacked layers in GO. GO comprises of secured structure of ‘GO sheets that are exceptionally hydrophilic nature [10, 11]. GO based semiconductor nanocomposites have been used in photo catalyst, its due to potential applications for solar energy converted to chemical energy [11–13]. GO based various semiconductor photocatalysts available in literature survey, so profoundly improve the reactant action for nature remediation and vitality application in need [14].

ZnO is a large band gap energy (3.32 eV), semiconductor metal oxide; it is broadly utilized as a part of the photocatalytic colour degradation of water purification technology [15–17]. ZnO is much better efficiency than TiO_2 under UV light and with high quantum efficiency of ZnO [18]. The ZnO doped with GO is upheld upgrading the photocatalytic synergist action, natural colour for electron replicated GO [19, 20]. Recently, GO based nanocomposite photocatalyst have been gained increasing attention, since they develop the charge transfer at the interface and have excellent adsorption capabilities for organic dye pollutants on their surfaces [21, 22]. Generally TiO_2 , ZnO, SiO_2 , and V_2O_5 semiconductor metal oxide electron hole recombination for valence band to the conduction band rather than the photo

✉ C. Pragathiswaran
pragathis_waran@yahoo.com

M. Chinnadurai
duraicd@gmail.com

¹ Department of Chemistry, Periyar E.V.R College
(Autonomous), Bharathidasan University, Tiruchchirappalli,
Tamil Nadu 620 023, India

² Department of Physics, Alagappa University, Karaikudi,
Tamil Nadu 630 003, India

generated active species for photocatalytic degradation of organic and inorganic dye [23]. The reaction was carried out with water, initiating redox reaction for the organic dye molecule adsorbed for catalyst on the surface. ZnO is more attractive towards UV light due to adsorbed, GO supported for highly electron hinder and positive charge carrier for the redox nature of composite materials in aqueous solution [24]. The GO/ZnO nanorods of various nanostructures and different substrate via seeded solution and the growth method of the thin film photoconductor, based on the ZnO/GO nanorods heterostructure is high sensitivity is visible light sensing [25, 26]. Under the visible light GO has electron transferring valence band property towards the conduction band ZnO and transferring ZnO is higher photo catalytic of chromium (VI) reduction [8].

The Ag NPs were synthesized and decorated on GO/ZnO nanocomposite poses spherical shape (GO/ZnO–Ag). The GO/ZnO–Ag nanocomposite annealing at 450 °C, the formation of spherical structure is transformed from GO nanosheets. The exhibit that covering GO/ZnO–Ag on GO significantly improves the photo induced charge-transfer effectiveness and electron-transfer rate, resulting in the superior photocatalytic activities. The GO/ZnO–Ag nanocomposite was according to the materials great attention of increasing surface area and enhancing the adsorptive of photocatalytic dye degradation. The GO/ZnO–Ag nanocomposite reaction were carried out in the aqueous solution medium in direct sunlight for RhB dye degradation, optimum level was happened at a brief time.

2 Materials and methods

2.1 Materials

All the chemicals were purchased from Sigma Aldrich Mumbai, India graphite powder (Sigma Aldrich 99.99 %), zinc sulphate ($\text{ZnSO}_4 \cdot 7\text{H}_2\text{O}$ 99.98 %), ammonium bicarbonate (NH_4HCO_3 99.99 %), silver nitrate (AgNO_3 99.98 %), sulphuric acid (H_2SO_4 98.00 %), hydrogen peroxide (H_2O_2 99.98 %), potassium permanganate (KMnO_4 99.97 %), sodium hydroxide (NaOH 99.98 %), sodium nitrate (NaNO_3 98.99 %) and sodium borohydride (NaBH_4 99.98 %) were received from Merck Chemicals. Absolute ethanol (EtOH), methanol (MeOH) and rhodamine B (Rh B) dye double distilled water were used through out the reaction for the preparation of aqueous solutions.

2.2 Synthesis of graphene oxide (GO)

GO was prepared from natural graphite powder through modified Hummers method [26, 29]. In a typical synthesis, 1 g of graphite powder was added in 23 ml of 98 %

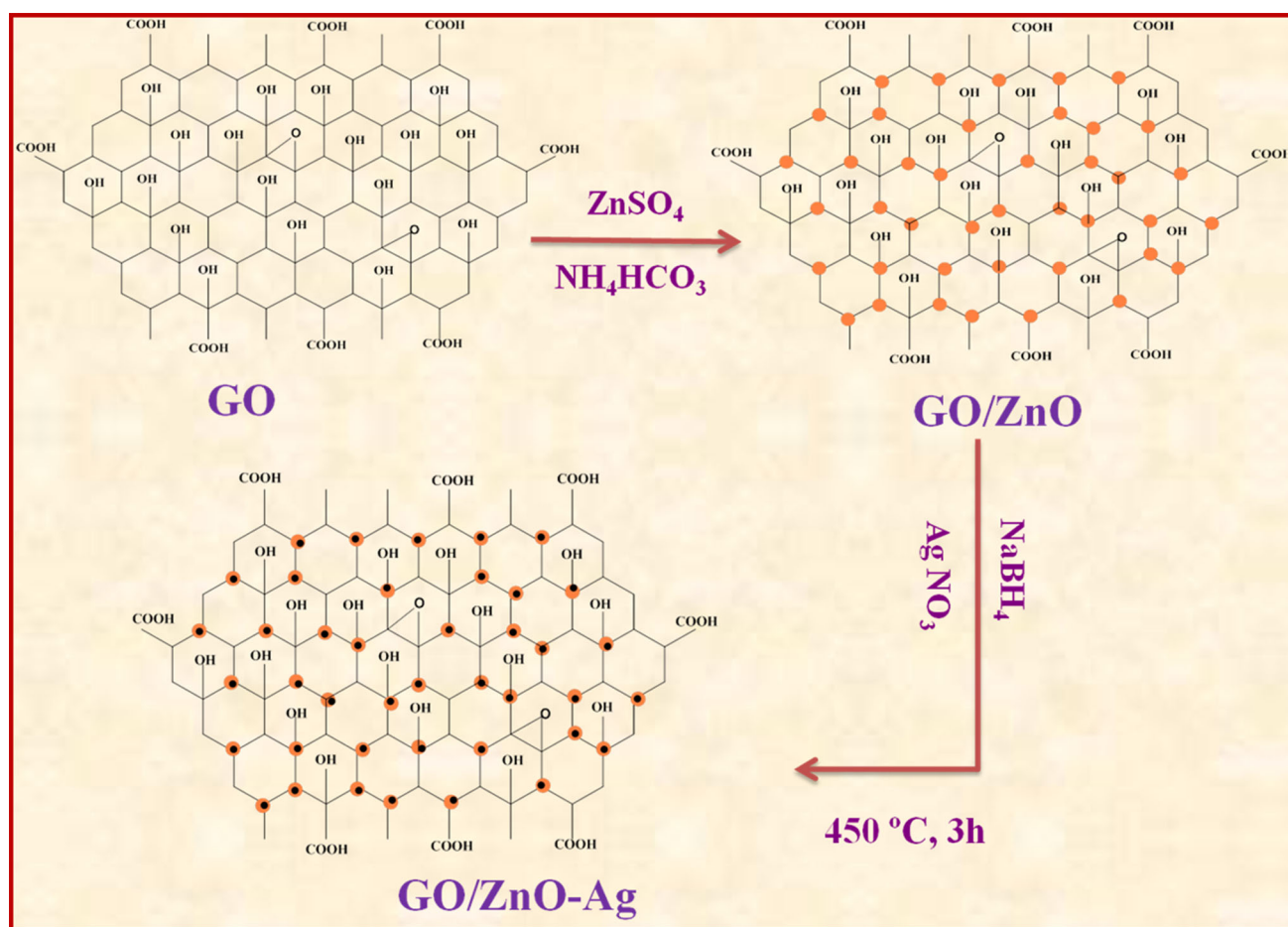
H_2SO_4 , followed by stirring at room temperature over a period of 24 h. After that, 100 mg of NaNO_3 was introduced into the mixture and stirred for 30 min. Subsequently, the mixture was kept below 5 °C by ice bath and 3 g of KMnO_4 was slowly added into the mixture. After heating 35–40 °C, the mixture was stirred for another 30 min. After 46 ml of water was added into the above mixture, by the period of 25 min. Finally, 140 ml of deionised double distilled water and 10 ml of H_2O_2 were added into the mixture to stop the reaction. After the reaction completes unexploited graphite in the resulting mixture was removed by centrifugation and the precipitate was collected and dried in hot air oven 100 °C end the product was calcinated at 400 °C for 3 h.

2.3 Preparation of GO/ZnO–Ag nanocomposite

1 g of GO and 50 ml of 1.0 M ZnSO_4 solution was added drop wise into 30 ml of 2.0 M NH_4HCO_3 solution under vigorous stirring at 60 °C in water bath for 1 h. The black precipitate was isolated by filter and washed for three times with double distilled water and ethanol, dried in a vacuum oven at 60 °C for 24 h. Finally, the product was calcined at 600 °C for 1 h to obtain black powder of GO/ZnO [34]. The Ag NPs were deposited on the surface of GO/ZnO nanocomposite through a chemical-reduction method, in which Ag^+ ions were converted into Ag NPs. In the typical synthesis, 1 g of the preformed GO/ZnO nanocomposite was dispersed in 250 ml of double distilled water with continuous stirring for 30 min to get a homogeneous distribution of GO/ZnO nanocomposite. The AgNO_3 (5 wt%) was added and stirred towards the reduction of Ag^+ ions upon the drop-wise addition of NaBH_4 until the colour changed to greenish yellow. The appearances of the greenish yellow colour indicate the formation of GO/ZnO nanocomposite and the solution was continuously stirred for another 30 min. The GO/ZnO–Ag nanocomposite was filtered, washed thoroughly with double distilled water, procured sample dried at 60 °C for 3 h and finally calcinated at 450 °C for 3 h (Scheme 1).

2.4 Characterization

The surface morphology studies for GO/ZnO–Ag nanocomposite was analysed by ZEISS Auriga field emission scanning electron microscope (FE-SEM) and energy dispersive X-ray spectroscopy (EDAX) was used to find out its elemental composition. Transmission electron microscope (TEM-H7650), powder X-ray diffraction (XRD) analysis of the samples were carried out on Scintag-XDS-2000 spectrometer with $\text{Cu K}\alpha$ radiation under applied voltage of 40 kV and current of 30 mA. The absorption spectrum of GO/ZnO–Ag catalyst was recorded



Scheme 1 Schematic illustration of the preparation procedure of GO/ZnO–Ag nanocomposite

using UV–Vis spectrophotometer (UV-2550, Shimadzu). A diffuse reflectance spectrum (DRS) of the nanocomposite was with an aid of using ISR-2200 DRS accessory of UV–Vis spectrophotometer (UV-2550, Shimadzu). Fourier transforms infrared spectroscopy (FT-IR) analysis of the functional group was performed (FT-IR Shimadzu-650) using KBr pellet disk.

2.5 Photocatalytic activity

Photocatalytic activities of GO, GO/ZnO and GO/ZnO–Ag nanocomposite were assessed by the degradation of rhodamine B dye under direct sunlight irradiation. The reaction cell was placed in a sealed black box with an opening on the top to provide visible-light irradiation. In a typical process, 100 mg of GO, GO/ZnO and GO/ZnO–Ag photocatalyst was independently included in 100 ml of RhB dye with a concentration of 10 mg l^{-1} . After the composite material is introduced into an ultrasonic bath for 5 min, the solution was stirred for 30 min in the dark to reach the adsorption/desorption equilibrium between the catalyst and the selected RhB dye. Then, the suspension was exposed to

the direct sunlight irradiation. The samples were collected at given regular time intervals and the dye concentration was measured by using UV–Vis spectroscopy.

3 Results and discussion

3.1 Surface morphology analysis (SEM)

The FE-SEM has been characterized for the morphology structure of GO, GO/ZnO and GO/ZnO–Ag nanocomposite as shown in the Fig. 1. It is conforms in which FE-SEM images reveal that the GO sheet are appeared in Fig. 1a. It's due to there is no agglomeration in the nanocomposite, implying that the ZnO can efficiently attach with GO. The reaction mechanisms of synthesis GO surface reaction by ZnO nucleus has been demonstrated by surface functional group interaction [28, 29, 31]. Figure 1b shows that the developing of ZnO revealed that the gathering of graphene sheets beside with the mineralized ZnO nanoparticles formation of the spherical structures. It can be clearly seen from FE-SEM images ZnO and Ag is well stacked on the

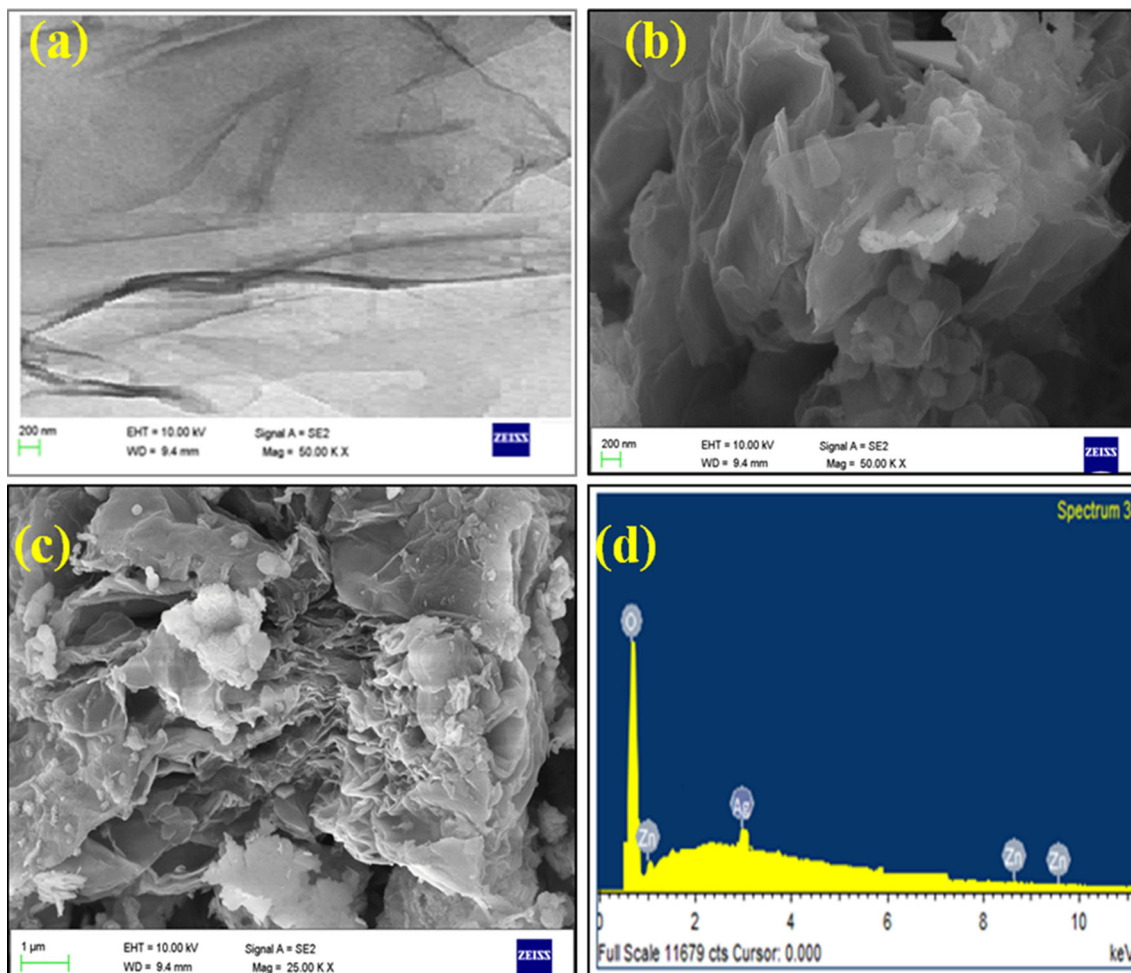


Fig. 1 SEM image of **a** GO, **b** GO/ZnO, **c** GO/ZnO–Ag nanocomposite

GO surface as shown in the Fig. 1c. The extremely closed to the graphene sheet so highly enhancing the photo catalytic activity for this composite. The elements were analyzed by EDAX spectrum; the C, Zn and Ag are apparently confirmed in the EDAX spectrum in Fig. 1d.

3.2 Transmission electron microscope (TEM)

The TEM morphology of the GO, GO/ZnO and GO/ZnO–Ag nanocomposite were characterized are shown in Fig. 2. In the TEM images reveal that the GO sheets GO is shown in Fig. 2a, the TEM image illustrates the exfoliated GO sheets. In the GO–ZnO, the mineralized ZnO nanoparticles are seen intertwined with the GO sheets to form near spherical shape aggregates in Fig. 2b [7, 27, 28]. It can be clearly seen from TEM images ZnO and Ag is well stacked on the GO surface as shown in Fig. 2c. The micrographs evidently indicate the formulated Zn and Ag NPs possess spherical shapes and the measured size are in the range from 20 to 50 nm and also the electrostatic attraction of

GO bounded with Zn and Ag NPs. It obviously observed the average size of ZnO and Ag NPs for 20–30 and 10–20 nm.

3.3 X-ray diffraction

The XRD spectra of the arranged GO, GO/ZnO and GO/ZnO–Ag nanocomposite are appeared in Fig. 3. The XRD pattern shows in Fig. 3a GO peak obtained 2θ value 26.30 and the crystal plane of (0 0 2) stack on the GO, Fig. 3b shows the marked diffraction peaks of GO/ZnO nanocomposite. It can be viewed as the peaks of known hexagonal structure [28–30]. The crystallography plane of GO/ZnO has place with the zinc wurtzite type of diffraction peaks at 2θ values 31.2, 34.1, 35.9, 47.6, 56.2, 62.2, 66.1, 67.9 and 68.9 corresponding to the crystal plane of (1 0 0), (0 0 2), (1 0 1), (1 0 2), (1 1 0), (1 0 3), (2 0 0), (1 1 2), and (2 0 1) were confirmed with JCPDS-card No.: 36-1451. The high intensity of (1 0 1) indicates the anisotropic nature and implies to the chosen direction of crystallites.

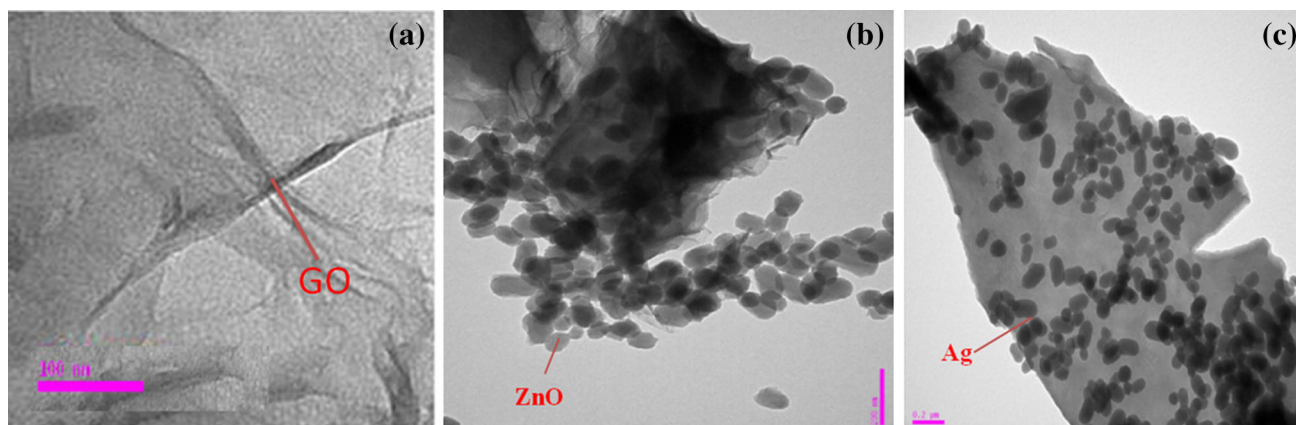


Fig. 2 TEM image of **a** GO, **b** GO/ZnO, **c** GO/ZnO–Ag nanocomposite

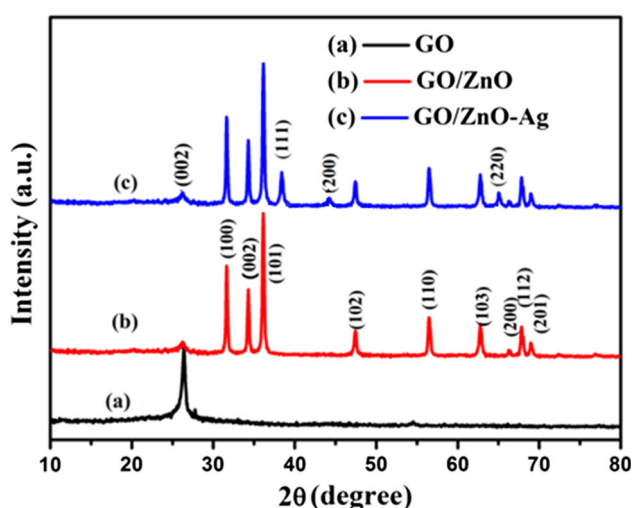


Fig. 3 XRD analysis of **a** GO, **b** GO/ZnO, **c** GO/ZnO–Ag nanocomposite

The XRD spectra in Fig. 3c differ from those of GO/ZnO and GO/ZnO–Ag nanocomposites. It can be observed that for the GO/ZnO–Ag composite, the three peaks at 2θ values of 38.3, 44.0, and 64.6 degrees, corresponding to the crystal planes (1 1 1), (2 0 0) and (2 2 0) were confirmed to the JCPDS card No: 08-7059 number crystal plane correspondingly. The crystalline size was calculated using Scherrer Eq. 1.

$$D = \frac{K\lambda}{\beta \cos\theta} \quad (1)$$

where λ is the wavelength of X-ray and β is the full width at half maximum, θ is the Bragg angle, K is the shape factor. The typical average crystalline size values for GO/ZnO–Ag and GO/ZnO nanocomposites are about 33.9 and 17.7 nm, respectively, computed from the intense peaks, which are available in the XRD pattern. The sharp peaks of the GO/ZnO–Ag nanocomposite indicate its extremely crystalline nature.

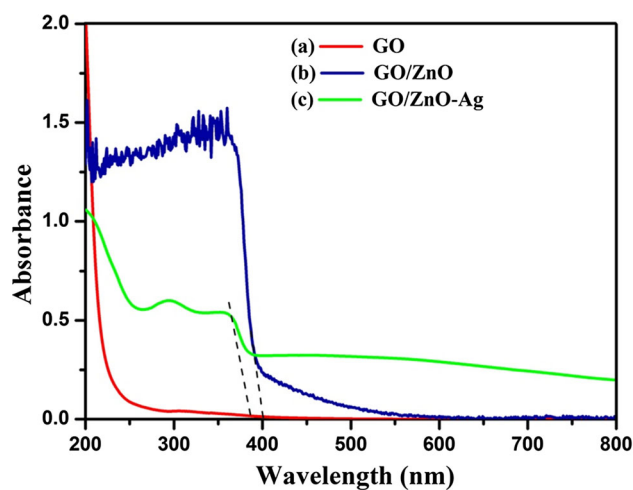


Fig. 4 The UV–visible diffuse reflectance spectra of **a** GO, **b** GO/ZnO, **c** GO/ZnO–Ag nanocomposite

3.4 UV–visible diffuse reflectance spectra

The UV–visible diffuse reflectance spectra of GO, GO/ZnO and GO/ZnO–Ag nanocomposites, which can be determined by the visible light absorption characteristics, are shown in Fig. 4. The wavelength dispersions of absorption light can be observed. The property of catalysis irradiation and quantum efficiency. GO/ZnO nanocomposite shows low photocatalytic activity due to its lower visible light absorbance. GO/ZnO–Ag nanocomposite shows higher photocatalytic activity towards Rh B due to the electron–hole recombination process. The absorbance peak of GO/ZnO–Ag and GO/ZnO nanocomposites are shown in Fig. 4, the absorption in the range of 290–400 nm in the visible region is caused by the surface plasma resonance peak, which confirms the presence of silver deposited on the catalyst surface. The energy band gap calculated for the Kubelka–Munk function effects for

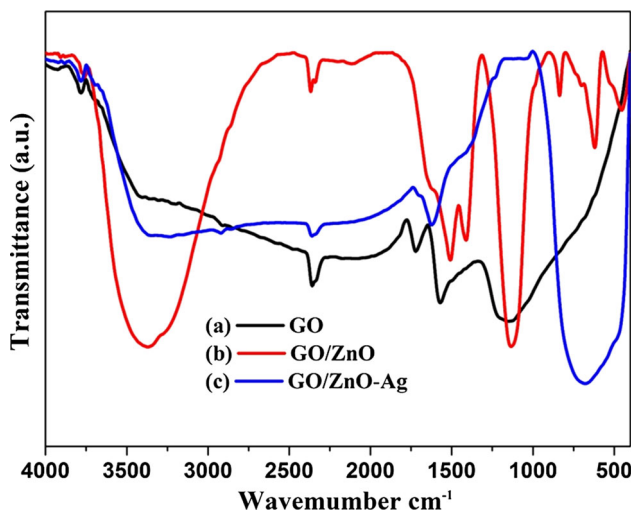


Fig. 5 The FT-IR spectra of **a** GO, **b** GO/ZnO, **c** GO/ZnO-Ag nanocomposite

evaluating energy band gap to the sample 3.24 and 3.13 eV subsequently to the GO/ZnO and GO/ZnO-Ag nanocomposite respectively [8, 28, 31].

3.5 FT-IR analysis

The FT-IR spectra of GO, GO/ZnO and GO/ZnO-Ag nanocomposite are appeared in Fig. 5. In the GO peaks at 1108, 1222, and 1731 cm^{-1} corresponding to the stretching of oxygen and carbon bonds are appeared in the Fig. 5a [23]. The FTIR regions of 1568 cm^{-1} suggestion to the vibration of the C-C bonding, O-H bending vibration to the epoxide group or O-H deformation, vibration -COOH group broad absorption band at 3454 cm^{-1} compared with the stretching vibration mode of -OH captivated water molecule. As shown in the Fig. 5b, attributed peak located at 450 cm^{-1} for to Zn-O [32, 33]. Among the GO/ZnO-Ag nanocomposite are shown in Fig. 5c, the presence of peaks at 1629 cm^{-1} may be corresponding to the vibration of the

C-C bond and regions for 1021 cm^{-1} symmetric and asymmetric stretching vibration of GO respectively.

3.6 Photocatalytic activity measurement

The photocatalytic preparations of GO, GO/ZnO and GO/ZnO-Ag nanocomposite are carried out for catalytic activity decomposition of rhodamine B in direct sunlight which is shown in Fig. 6. In the GO, GO/ZnO and GO/ZnO-Ag nanocomposite are evaluated by photocatalytic degradation of RhB in aqueous solution under direct sunlight irradiation by monitoring the intensity of the characteristic absorption peak at 525 nm for RhB. The expert degradation by a photocatalyst in aqueous solution depends upon its capability of absorbing light and its low rate of recombination of electron-hole pair [34–36]. This ability promotes the production of oxidizing hydroxyl (OH·) radicals that requires appropriate band gap energy compared to that of incident photons. To improve the production of hydroxyl radicals is dependent on charge carrier recombination rate [28, 29, 31]. They GO/ZnO-Ag nanocomposite extensively improves the photo induced charge-transfer efficacy and electron-transfer rate, ensuing in the better photo catalytic activities nanocomposite. Absorption spectrum changes in according to the photodegradation of RhB. The GO/ZnO-Ag nanocomposites, it has been found that a strong hybridization interaction between ZnO-Ag and GO. The development of the C-O bonds can decrease the activation of the surface oxygen atom of GO/ZnO-Ag and lead to the improvement of photo stability, thus, the photo stability of GO/ZnO-Ag has been greatly improved [35–38]. From the Catalytic activity study, it is observed that while irradiation time increases, the concentration of RhB dye is decreased and UV-visible region absorption intensity peaks are also decreased. Photocatalytic efficiency (or) efficacy of GO, GO/ZnO and GO/ZnO-Ag nanocomposites under the reaction directs sunlight 73, 78 and 94 % RhB dye degradation respectively are shown in Fig. 6. This show the performances of GO/

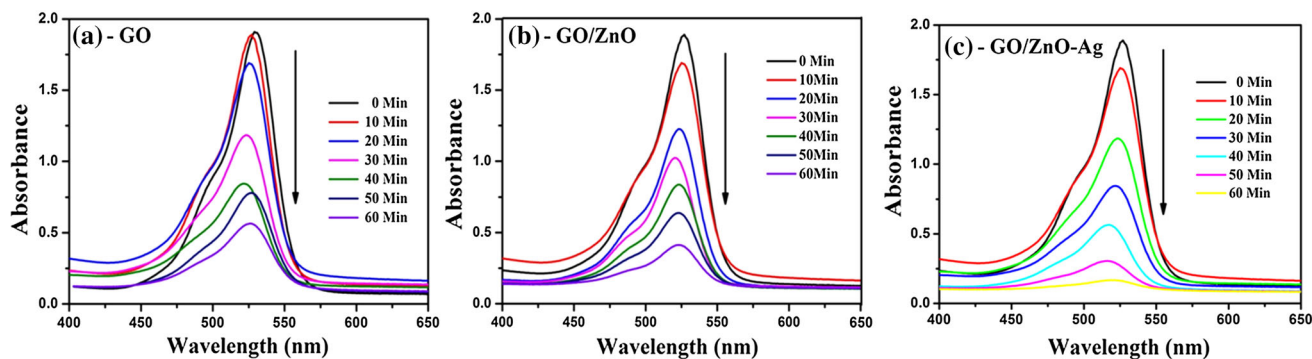


Fig. 6 The UV-visible spectra of Photo catalytic activity for **a** GO, **b** GO/ZnO, **c** GO/ZnO-Ag nanocomposite

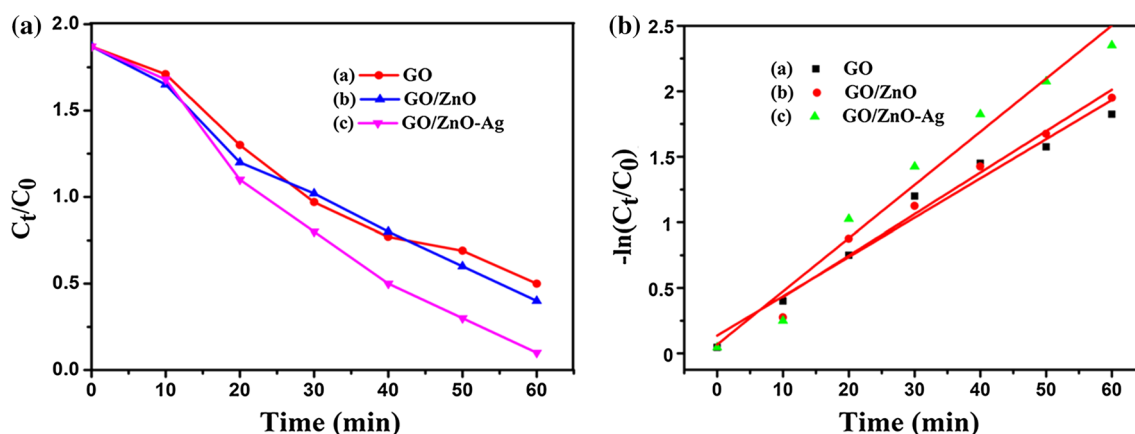


Fig. 7 **a** UV–visible Photocatalytic degradation of Rh B dye, **b** UV–visible photocatalytic degradation of Rh B kinetics rate constant with different nanocomposite

ZnO–Ag nanocomposite are effective and highly illuminate towards the catalytic degradation of dye.

The photocatalytic degradation of RhB dye with GO, GO/ZnO and GO/ZnO–Ag nanocomposite is shown in Fig. 7. Normally the photocatalytic degradation of organic dyes by semiconductor under light irradiation generally involves the excitation to the semiconductor to form photo generated (e^- , h^+) pairs and subsequent chemical reactions, with the surrounding media after the photo generated holes move to the particle surface and react with organic dye molecules to form CO_2 and H_2O . The other possible mechanism is based on the excitation of dye in which the dye acts as a sensitizer under visible light as well as infuses excited electrons to an electron acceptor to become a cationic dye radical (dye^{*+}), followed by self-degradation of dye molecules.

The kinetics of photo catalytic dye degradation of RhB was studied and carried out with the experimental optimum condition for the concentration of 10 mg l^{-1} . Catalyst dosage for 0.1 g l^{-1} irradiation of adsorption desorption equilibrium time at 60 min [7, 29, 39–42]. In the experiment catalytic degradation where obeys the pseudo first order kinetics rate constant [plots $-\ln(C/C_0)$] verses to the time show linear relationship where C is the concentration of RhB dye [36, 37]. The integration limit of C/C_0 at $t = 0$ with C_0 is the equilibrium concentration bulk solution of RhB dye. The equation $[\ln(C/C_0) = kt]$, where C_0 is the equilibrium concentration of the dye solution and C is a concentration at time t. When this Eq. 2.

$$\ln\left(\frac{C_0}{C}\right) = K_{\text{App}}t \quad (2)$$

K_{App} is the apparent first order kinetics of the rate constant (min^{-1}). The rate constant value for photocatalytic degradation of RhB dye was determined GO, GO/ZnO and

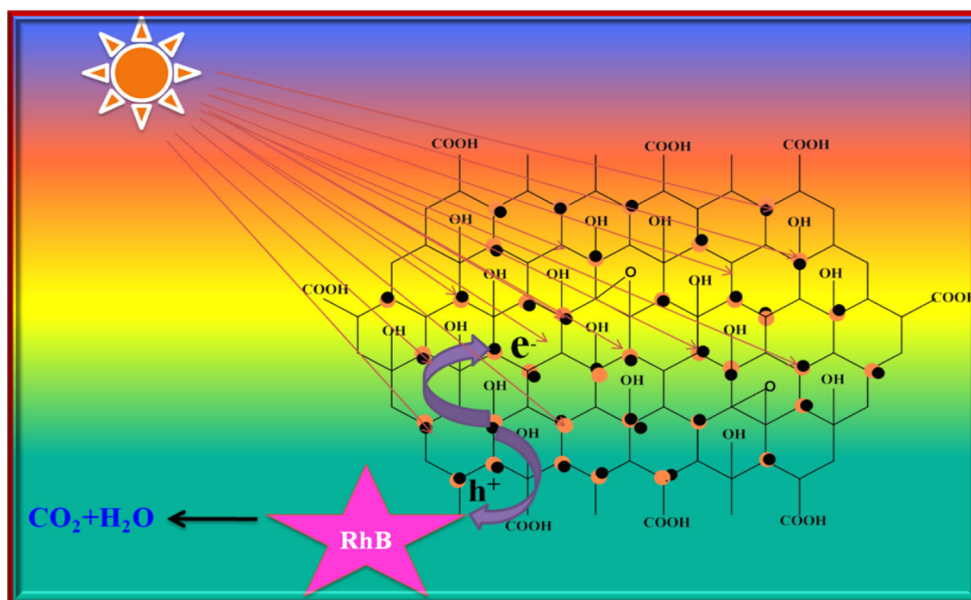
GO/ZnO–Ag to be $k = 1.1978$, $k = 1.2657$ and $k = 1.6228 \text{ min}^{-1}$ respectively.

3.7 Mechanism of photocatalytic activity

The proposed mechanism for photocatalytic degradation of RhB dye, over GO/ZnO–Ag nanocomposite was proposed as shown in Fig. 8. The UV–visible light irradiation, the electrons in the valence band of GO/ZnO–Ag nanocomposite can be excited to the conduction band, departure holes in the valence band. After that, the photogenerated electrons can move to GO due to the interfacial contact between GO/ZnO and Ag nanocomposites [8, 22]. The GO which hinders the recombination of electrons and holes efficiently. The RhB molecules can be moved from the solution to the surface of the nanocomposite and adsorbed with counter face-to face way conjugation among RhB and aromatic regions of GO as evidenced by the superior adsorptive of RhB over GO/ZnO–Ag nanocomposite.

The adsorbed RhB can be oxidized by the hole directly and the photoactive radicals (e.g. hydroxyl radicals and superoxide radicals) generated in the photocatalytic reaction to produce CO_2 and H_2O other mineralized intermediates [7, 31]. On the basis of above discussion, the most important effect of the addition of an appropriate quantity of GO in the nanocomposite of GO/ZnO–Ag nanocomposite can be summarized as follows. (1) The better adsorptive of RhB dye, can be ascribed to the accumulation of GO, which can lead to enhancement in the pore volume and size and adsorb RhB conjugation between RhB and aromatic regions of graphene. (2) The existence and transfer of photogenerated electron–hole pairs is superior because GO serves as an excellent supporting material for GO/ZnO–Ag and an electron acceptor or carrier, capably separate the photogenerated electron–hole pairs. This two

Fig. 8 Schematic diagram illustrating the charge-transfer process in the GO/ZnO–Ag nanocomposite



factors included in a proper synergistic performance in the account of enhanced observation of the photocatalytic activity of GO/ZnO–Ag nanocomposite as compared with GO/ZnO and GO toward degradation of RhB under ambient conditions.

4 Conclusion

The successful synthesis was GO/ZnO–Ag nanocomposite, the Ag present in the catalyst shows conformed for the XRD and TEM. The XRD result indicates for high crystalline size 33.9 nm. Due to this nanocatalyst small particle size photocatalytic activity of GO/ZnO–Ag nanocomposite has been enhanced. Thus, the most excellent photocatalytic performance of GO/ZnO–Ag nanocomposite results from in cooperation effective photo induced charge transfer and excellent adsorption ability toward RhB dye. This nanocomposites also can be used for degrade the other environment remediation.

Acknowledgments C. Pragathiswaran gratitude to the Staff Members, Department of Chemistry, Periyar E.V.R. College (Autonomous), Triuchirappalli-23. The author, P. Govindhan thanks the Branch Manager, Syndicate Bank, Matalampatti, Dharmapuri, sanctioning for education loan to conduct for their support to carry out this research work.

References

1. N. Zhang, M.Q. Yang, S. Liu, Y. Sun, Y.J. Xu, Chem. Rev. **115**, 10307–10377 (2015)
2. Q. Xiang, J. Yu, M. Jaroniec, Chem. Soc. Rev. **41**, 782–796 (2012)
3. F. Li, X. Jiang, J. Zhao, S. Zhang, Nano Energy **16**, 488–515 (2015)
4. K.S. Novoselov, A.K. Geim, S.V. Morozov, D. Jiang, Y. Zhang, S.V. Dubonos, I.V. Grigorieva, A.A. Firsov, Science **306**, 666–669 (2004)
5. X. Huang, X. Qi, F. Boey, H. Zhang, Chem. Soc. Rev. **41**, 666–686 (2012)
6. X. Huang, Z. Yin, S. Wu, X. Qi, Q. He, Q. Zhang, Q. Yan, F. Boey, H. Zhang, Small **7**, 1876–1902 (2011)
7. Y. Zhang, S. Liu, L. Wang, X. Qin, J. Tian, W. Lu, G. Chang, X. Sun, RSC Adv. **2**, 538–545 (2012)
8. M.Q. Yang, Y.J. Xu, J. Phys. Chem. C **117**, 21724–21734 (2013)
9. W. Shao, X. Liu, H. Min, G. Dong, Q. Feng, S. Zuo, ACS Appl. Mater. Interfaces **7**, 6966–6973 (2015)
10. X.Y. Yang, X. Dou, A. Rouhanipour, L.J. Zhi, H.J. Rader, K. Mullen, J. Am. Chem. Soc. **130**, 4216–4217 (2008)
11. A. Buchsteiner, A. Lerf, J. Pieper, J. Phys. Chem. B **110**, 22328–22338 (2006)
12. Q. Xiang, J. Yu, J. Phys. Chem. Lett. **4**, 753–759 (2013)
13. Q. Xiang, J. Yu, M. Jaroniec, J. Phys. Chem. C **115**, 7355–7363 (2011)
14. W.J. Ong, S.Y. Voon, L.L. Tan, B.T. Goh, S.T. Yong, S.P. Chai, Ind. Eng. Chem. Res. **53**, 17333–17344 (2014)
15. R. Bera, S. Kundu, A. Patra, ACS Appl. Mater. Interfaces **7**, 13251–13259 (2015)
16. X. Wang, X. Wan, X. Xu, X. Chen, Appl. Surf. Sci. **321**, 10–18 (2014)
17. D. Pan, J. Jiao, Z. Li, Y. Guo, C. Feng, Y. Liu, L. Wang, M. Wu, ACS Sustain. Chem. Eng. **3**, 2405–2413 (2015)
18. D.H. Yoo, T.V. Cuong, V.H. Luan, N.T. Khoa, E.J. Kim, S.H. Hur, S.H. Hahn, J. Phys. Chem. C **116**, 7180–7184 (2012)
19. T. Bharathidasan, A. Mandalam, M. Balasubramanian, P. Dhandapani, S. Sathiyarayanan, S. Mayavan, ACS Appl. Mater. Interfaces **7**, 18450–18459 (2015)
20. N.P. Herring, S.H. Almahoudi, C.R. Olson, M.S. El-Shall, J. Nanopart. Res. **14**, 1277–1289 (2012)
21. Y. Liao, C. Xie, Y. Liu, H. Chen, H. Li, J. Wu, Ceram. Int. **1**, 4437–4444 (2012)
22. M.Q. Yang, N.Y. Zhang, M. Pagliaro, Y.J. Xu, Chem. Soc. Rev. **43**, 8240–8254 (2014)
23. N. Zhang, Y. Zhang, Y.J. Xu, Nanoscale **4**, 5792–5813 (2012)

24. C. Justin Raj, K. Prabakar, S.N. Karthick, K.V. Hemalatha, M.K. Son, H.J. Kim Banyan, *J. Phys. Chem. C* **117**, 2600–2607 (2013)
25. K. Vignesh, S. Kang, B.S. Kwak, M. Kang, *Sep. Purif. Technol.* **147**, 257–265 (2015)
26. Z. Chen, N. Zhang, Y.J. Xu, *CrystEngComm* **15**, 3022–3030 (2013)
27. T.N. Reddy, J. Manna, R.K. Rana, *ACS Appl. Mater. Interfaces* **7**, 19684–19690 (2015)
28. N.T. Khoa, S.W. Kim, D.H. Yoo, S. Cho, E.J. Kim, S.H. Hahn, *ACS Appl. Mater. Interfaces* **7**, 3524–3531 (2015)
29. J. Xu, H. Sang, X. Wang, K. Wanga, *Dalton Trans.* **44**, 9528–9537 (2015)
30. N. Yang, Y. Liu, H. Wen, Z. Tang, H. Zhao, Y. Li, D. Wang, *ACS Nano* **7**, 1504–1512 (2013)
31. S. Wi, H. Woo, S. Lee, J. Kang, J. Kim, S. An, C. Kim, S. Nam, C. Kim, B. Park, *Nanoscale Res. Lett.* **10**, 204 (2015)
32. R. Saravanan, M.M. Khan, V.K. Gupta, E. Mosquera, F. Gracia, V. Narayanan, A. Stephen, *RSC Adv.* **5**, 34645–34651 (2015)
33. S. Thangavel, K. Krishnamoorthy, V. Krishnaswamy, N. Raju, S. Jae Kim, G. Venugopal, *J. Phys. Chem. C* **119**, 22057–22065 (2015)
34. X. Liu, L. Pan, Q. Zhao, T. Lv, G. Zhu, T. Chen, T. Lu, Z. Sun, C. Sun, *Chem. Eng. J.* **183**, 238–243 (2012)
35. W.N. Wang, J. Park, P. Biswas, *Catal. Sci. Technol.* **1**, 593–600 (2011)
36. S.A. Ansari, M.M. Khan, M.O. Ansari, J. Lee, M.H. Cho, *J. Phys. Chem. C* **117**, 27023–27030 (2013)
37. C. Han, M.Q. Yang, B. Weng, Y.J. Xu, *Phys. Chem. Chem. Phys.* **16**, 16891–16903 (2014)
38. O. Akhavan, *ACS Nano* **4**, 4174–4180 (2010)
39. G.R. Xu, J.N. Wang, C.J. Li, *Appl. Surf. Sci.* **279**, 103–108 (2013)
40. A. Maleki, M. Safari, B. Shahmoradi, Y. Zandsalimi, H. Daraei, F. Gharibi, *Environ. Sci. Pollut. Res.* **22**, 16875–16880 (2015)
41. S. Safa, R. Sarraf-Mamssoory, R. Azimirad, *J. Sol Gel Sci. Technol.* **74**, 499–506 (2015)
42. Y. Zhang, S. Zhang, M. Zheng, H. Pang, *Int. J. Electrochem. Sci.* **10**, 8706–8713 (2015)
43. J.P. Dhal, B.G. Mishra, G. Hota, *RSC Adv.* **5**, 58072–58083 (2015)
44. H.Y. He, J. Fei, J. Lu, *Micro Nano Lett.* **10**, 389–394 (2015)